A Nanoscale Optical Biosensor: Real-Time Immunoassay in Physiological Buffer Enabled by Improved Nanoparticle Adhesion

Jonathan C. Riboh,† Amanda J. Haes,† Adam D. McFarland, Chanda Ranjit Yonzon, and Richard P. Van Duyne*

Department of Chemistry, Northwestern University, Evanston, Illinois 60208-3113

Received: September 24, 2002; In Final Form: December 9, 2002

The shift in the extinction maximum, λ_{max}, of the localized surface plasmon resonance (LSPR) spectrum of triangular Ag nanoparticles (~90 nm wide and 50 nm high) is used to probe the interaction between a surface-confined antigen, biotin (B), and a solution-phase antibody, anti-biotin (AB). Exposure of biotin-functionalized Ag nanotriangles to 7×10^{-7} M < [AB] < 7×10^{-6} M caused a ~38 nm red-shift in the LSPR λ_{max}. The experimental normalized response of the LSPR λ_{max} shift, ($\Delta R/\Delta R_{max}$), versus [AB] was measured over the concentration range 7×10^{-10} M < [AB] < 7×10^{-6} M. Comparison of the experimental data with the theoretical normalized response for a 1:1 binding model yielded values for the saturation response, $\Delta R_{max} = 38.0$ nm, the surface-confined thermodynamic binding constant, $K_{a,surf} = 4.5 \times 10^7$ M^{-1}, and the limit of detection (LOD) < 7×10^{-10} M. The experimental saturation response was interpreted in terms of a closest-packed structural model for the surface B−AB complex in which the long axis of AB, $l_{AB} = 15$ nm, is oriented horizontally and the short axis, $h_{AB} = 4$ nm is oriented vertically to the nanoparticle surface. This model yields a quantitative response for the saturation response, $\Delta R_{max} = 40.6$ nm, in good agreement with experiment, $\Delta R_{max} = 38.0$ nm. An atomic force microscopy (AFM) study supports this interpretation. In addition, major improvements in the LSPR nanobiosensor are reported. The LSPR nanobiosensor substrate was changed from glass to mica, and a surfactant, Triton X-100, was used in the nanosphere lithography fabrication procedure. These changes increased the adhesion of the Ag nanotriangles by a factor of 9 as determined by AFM normal force studies. The improved adhesion of Ag nanotriangles now enables the study of the B−AB immunoassay in a physiologically relevant fluid environment as well as in real-time. These results represent important new steps in the development of the LSPR nanosensor for applications in medical diagnostics, biomedical research, and environmental science.

I. Introduction

Noble metal nanoparticles have extraordinary, size-dependent optical properties that have recently been the subject of extensive studies.[1−10] These nanoparticles exhibit a strong UV−vis absorption band that is not present in the spectrum of the bulk metal.[11−19] This absorption band results when the incident photon frequency is resonant with the collective excitation of the conduction electrons and is known as the localized surface plasmon resonance (LSPR).[11−18,20] LSPR excitation results in wavelength selective absorption with extremely large molar extinction coefficients ~3×10^{11} M^{-1} cm^{-1},[20] resonant Rayleigh scattering[21,22] with an efficiency equivalent to that of 10^6 fluorophors,[23,24] and enhanced local electromagnetic fields near the surface of the nanoparticle which are responsible for the intense signals observed in all surface-enhanced spectroscopies.[25] It is well established that the peak extinction wavelength, λ_{max}, of the LSPR spectrum is dependent upon the size, shape, and interparticle spacing of the nanoparticle as well as its own dielectric properties and those of its local environment including substrate, solvent, and adsorbates.[11−19] The high sensitivity of the LSPR spectrum of nonspherical nanoparticles to adsorbate-induced changes in the local dielectric constant (viz., refractive index) are now being used to develop a new class of nanoscale chemosensors and biosensors.

There is significant demand for the development of simple, robust, and accurate biosensors for deployment in a broad range of applications such as the diagnosis and monitoring of diseases, drug discovery, proteomics, and the environmental detection of biological agents.[26] Optical biosensors, in particular, have found a broad range of applications in the detection of many biological molecules such as glucose,[27] DNA,[28] *E. coli*,[29,30] anthrax,[31] and other proteins.[32] A field of particular interest is the study of the interaction between antigens and antibodies.[33] For these reasons we have chosen to focus the present LSPR nanobiosensor study on the prototypical immunoassay involving biotin (B) and anti-biotin (AB).

AB, as used in this study, is a member of the large immunoglobulin superfamily.[35] The common structural feature among these molecules is that they all contain the same subunit, the immunoglobulin fold.[35] An IgG antibody, such as the AB used in our study, consists of 12 immunoglobulin fold subunits, folded into a Y-shaped three-dimensional structure. At the base of the Y is the constant fragment (Fc) which is common to all IgG molecules. Each arm of the Y contains a constant region and a variable region which is called the antigen binding fragment (Fab). AB can bind to surface B at both of its Fab sites, making it possible for a single AB molecule to attach to two surface-bound B molecules. No crystal structure has been

* Author to whom correspondence should be addressed. E-mail: vanduyne@chem.northwestern.edu.

† These authors contributed equally to this work.

10.1021/jp022130v CCC: $25.00
Published on Web 01/29/2003

determined for AB; however, the crystal structure for human IgG is available.[36] Since the Fab segment is the only structural unit that varies from one IgG to the next, it is assumed that the overall 3D structure of AB can be well approximated by that for human IgG.

Advances have been made in the detection of antigen−antibody interactions, using methods as diverse as light scattering,[37] surface plasmon resonance (SPR) sensors,[38,39] nanowire electrical sensors,[40] and observation of the orientation of IgG modified liquid crystals on a biotinylated surface.[41] It has also been shown that equilibrium and kinetic binding measurements of the antigen−antibody interaction can be probed with SPR[42] and fluorescent labeling.[43] The LSPR nanobiosensor discussed in this paper combines the benefits of all these methods. It can detect the real time equilibrium kinetics of AB to B and provide specific binding information for this couple. Furthermore, it offers the advantage of a simple, cost-effective experimental setup which can be miniaturized in theory to a ∼100 nm detector.

While several types of biosensors exist,[44−59] this study focuses on an optical biosensor that detects changes in local refractive index by monitoring the LSPR λ_{max} extinction maximum with UV−vis spectroscopy. Currently, the most widely used optical biosensor is the SPR sensor. This sensor detects changes in the refractive index induced by molecules near the surface of noble metal thin films.[60] While demonstrating a broad range of applications, these systems would be difficult to transfer to a living medium because of their large size restrictions.[61−63] The LSPR sensor, the nanoparticle equivalent of the SPR sensor, provides an outlet to this difficulty. LSPR sensors could, in theory, be reduced to chips as small as 100 nm, using single nanoparticle spectroscopic techniques. Presently, the smallest immunosensor is a miniature SPR imaging sensor, whose dimensions are −500 μm × 500 μm.[64] Thus, the LSPR biosensor offers an exciting alternative to currently existing immunosensors. The advantages for in vivo applications are evident. The sensor would be completely noninvasive and would be capable of organelle specific sensing. LSPR biosensors offer a variety of advantages over traditional flat surface SPR due to the short electromagnetic field decay length (∼5−6 nm)[65] of noble metal nanoparticles.

In previous work, Van Duyne et al. measured the short-range distance dependence of the LSPR extinction maximum of Ag nanoparticles synthesized using nanosphere lithography (NSL) via three pathways. First, systematic studies demonstrated that the LSPR extinction maximum, λ_{max}, of triangular Ag nanoparticles was so sensitive to the presence of alkanethiol adsorbates that it exhibited a linear red-shift corresponding to 3.3 nm for every carbon atom in the alkane chain accompanied by an 8.5 nm blue-shift due to the Ag−S charge-transfer interaction.[44] As an additional proof of concept, it was shown that the LSPR λ_{max} reversibly red-shifted by ∼5 nm in response to the electrostatic adsorption of the polypeptide poly-L-lysine to Ag nanoparticles modified with deprotonated carboxylate groups from 11-mercaptoundecanoic acid (11-MUA).[44] Finally, it was shown that the LSPR nanosensor could be used to detect <1 pM streptavidin to biotinylated Ag nanoparticles with almost no nonspecific binding effects.[45]

In this study, we report the use of Ag nanotriangles synthesized using NSL[66] as a LSPR biosensor that monitors the interaction between a biotinylated surface and free AB in solution. The importance of this study is that it demonstrates the feasibility of LSPR biosensing with a biological couple whose binding affinity is significantly lower ($1.9 \times 10^6 - 4.98 \times 10^8$ M^{-1})[37,39] than in previously studied models.[45] In our previous LSPR biosensor studies, the biotin−streptavidin model demonstrated that LSPR biosensing was possible.[45] This study expands on that previous work and also demonstrates the use of LSPR nanobiosensing under biologically relevant conditions. While this LSPR biosensor functions analogously to the one used for the streptavidin model, differences were noticed and improvements were made to its setup. Namely, changes were seen in the maximum LSPR response, as expected since this depends on the size and density of the analyte molecule; the surface binding affinity for the AB/B pair; and the limit of detection of the biosensor (directly dependent on the binding affinity constant). The maximum LSPR wavelength shift observed for AB binding to biotinylated nanoparticles was $\Delta\lambda_{max} = +38.0$ nm (the + sign indicates a red-shift). Fits to the experimental data revealed a surface binding affinity of 4.5×10^7 M^{-1} for the binding of AB to the biotinylated Ag nanoparticles. Finally, the limit of detection for the biosensor was determined to be less than 700 pM AB, which as predicted, is higher than that observed for streptavidin which interacts very strongly with B.[45]

Furthermore, we have considerably optimized the LSPR biosensor design. First, the NSL sphere packing technique has been modified by changing the sample substrate from glass to mica and by adding a surfactant, Triton X-100 and methanol (1:400 by volume) in a 1:1 ratio to the sphere solution before drop coating. The resulting surface area of a perfect single-layer sphere monolayer is increased, and as a result, the number of monodisperse Ag nanoparticles in that area is increased. The change in substrate and the use of a surfactant have also dramatically improved the adhesion of the Ag nanoparticles to the sensor substrate. It will be shown that a normal force of 10 nN, as determined by atomic force microscopy (AFM), was sufficient to remove all Ag nanoparticles from a glass surface. By performing the force measurements on mica substrates where no surfactant was used, it was revealed that the normal force required to remove the nanoparticles increased to 50 nN. The mechanical stability, or adhesion of the nanoparticles onto mica, increased even further to 90 nN of normal force when Triton X-100 was used during sphere packing. The LSPR biosensor now fulfills two major prerequisites for biological studies; that is, it is robust and durable. Two additional factors that are indispensable for in vivo use of a nanobiosensor are effectiveness under physiological conditions and reusability. We demonstrate that for the AB/B model, the LSPR biosensor works in 10 mM phosphate buffered saline (PBS), a close emulate of physiological fluids,[67] with a loss of sensitivity less than that expected from theoretical studies.[45] Finally, it will be shown that by treating samples that have AB on them with an excess of concentrated B, the binding of AB to the biotinylated Ag nanoparticles can be completely reversed, rendering the sample reusable. These results, in combination with previous studies that indicated that the LSPR nanobiosensor reacts minimally to nonspecific binding,[45] offer an exciting application of nanoscience to medical diagnostics and biomedical research.

The LSPR nanobiosensor developed in this study is expected to demonstrate a wide range of biomedical and environmental applications. Presently, work is being done to miniaturize the LSPR biosensor to monitor single molecule binding events on single nanoparticles.[68] Increasing the speed of adsorption and desorption of the analyte to the biotinylated surface would offer the possibility of real time concentration monitoring. While the commercially available SPR biosensor has some of these capabilities, a nanoparticle-based biosensor could improve both

medical diagnostics and biomedical research by easily diagnosing large numbers of biomolecules quickly.

II. Experimental and Methods

Materials. 11-MUA and 1-octanethiol (1-OT) were purchased from Aldrich (Milwaukee, WI). Hexanes and methanol were purchased from Fisher Scientific (Pittsburgh, PA). Polyclonal AB immunospecific to B as determined by immunoelectrophoresis, 10 mM and 20 mM phosphate buffered saline (PBS), pH = 7.4, were obtained from Sigma (St. Louis, MO). (+)-Biotinyl-3,6-dioxaoctanediamine (B) and 1-ethyl-3-[3-dimethylaminopropyl]carbodiimide hydrochloride (EDC), was purchased from Pierce (Rockford, IL). Absolute ethanol was purchased from Pharmco (Brookfield, CT). Ag wire (99.99%, 0.5 mm diameter) was obtained from D. F. Goldsmith (Evanston, IL). Tungsten vapor deposition boats were acquired from R. D. Mathis (Long Beach, CA). Polystyrene nanospheres with diameters of 390 nm ± 19.5 nm were received as a suspension in water (Duke Scientific, Palo Alto, CA). Triton X-100 was purchased from Aldrich (Milwaukee, WI). Millipore cartridges (Marlborough, MA) were used to purify water to a resistivity of 18 MΩ cm^{-1}. Ruby red muscovite mica substrates were purchased from Asheville-Schoonmaker Mica Co. (Newport News, VA). Borosilicate glass substrates with 18 mm diameters were obtained as Fisherbrand No. 2 cover slips (Fisher Scientific, Pittsburgh, PA).

Substrate Preparation. Mica substrates with 0.003" thickness were cut into circles of ~18 mm diameter. The samples were freshly cleaved immediately before use. Glass substrates were cleaned in piranha solution (1:3 30% H_2O_2/H_2SO_4) for 30 min at 80 °C. Samples were allowed to cool and were then rinsed profusely with water. Samples were then sonicated in 5:1:1 $H_2O/NH_4OH/30\%$ H_2O_2 and rinsed with water. The samples were stored in water until used.

Nanoparticle Preparation. NSL was used to fabricate monodisperse, surface-confined triangular Ag nanoparticles. A solution of nanospheres was drop coated onto a clean substrate and allowed to self-assemble into a 2D hexagonally close packed array that served as a deposition mask. On mica, the original nanosphere solution was diluted as a 1:1 solution with Triton X-100 and methanol (1:400 by volume). Approximately 4 μL of this solution produced large areas of single-layer colloidal crystal nanosphere masks. The surfactant allowed for better packing of the nanospheres on the mica surface. For AFM adhesion studies, single-layer colloidal crystal nanosphere masks were prepared by drop coating ~2 μL of undiluted nanosphere solution on glass and mica substrates. The samples were then mounted into a Consolidated Vacuum Corporation vapor deposition chamber system. A Leybold Inficon XTM/2 quartz crystal microbalance (East Syracuse, NY) was used to monitor the thickness of the Ag film deposited on the nanosphere mask. All samples in this study were covered with 50.0 nm thickness Ag films. Following Ag vapor deposition, the nanosphere mask was removed by sonicating the samples in ethanol for 3 min.

Nanoparticle Functionalization. First, the nanoparticle samples were placed directly in 1 mM 3:1 OT/MUA (ethanol) for 24 h. After incubation, the samples were rinsed with ethanol to remove physisorbed alkanethiol molecules and dried with N_2. Next, 1 mM B in 10 mM PBS was covalently linked to the surface carboxyl groups using EDC coupling over a 3 h period. Samples were rinsed with 10 mM PBS, 20 mM PBS, and water to remove electrostatically bound molecules. Following thorough rinsing and N_2 drying, the samples were incubated in AB solutions in 10 mM PBS for 3 h.

Ultraviolet−Visible Extinction Spectroscopy. Macroscale UV−vis extinction measurements were collected using an Ocean Optics (Dunedin, FL) SD2000 fiber optically coupled spectrometer with a CCD detector. All spectra in this study are macroscopic measurements performed in standard transmission geometry with unpolarized light. The probe diameter was approximately 4 mm. A home-built flow cell[44] was used to control the external environment of the Ag nanoparticle substrates. Because the raw spectra have a mica-induced interference pattern superimposed on the UV−vis spectra, all data presented here have been smoothed. The extinction maximum of each spectrum was located by calculating its first derivative.

Atomic Force Microscopy (AFM). A Digital Instruments Nanoscope IV microscope with a Nanoscope IIIa controller operating in either contact or tapping mode was used to collect AFM images in ambient conditions. In tapping mode, etched Si nanoprobe tips (TESP, Digital Instruments, Santa Barbara, CA) were used. These tips had resonance frequencies between 280 and 320 kHz and are conical in shape, with a cone angle of 20° and an effective radius of curvature at the tip of 10 nm. In contact mode, etched Si tips (Digital Instruments, Santa Barbara, CA) with spring constants of approximately 0.15 N m^{-1} were used. With the exception of Figure 6B, all images shown are unfiltered data that were collected in ambient conditions. Figure 6B was filtered to improve the quality of the image. The force constant of the AFM cantilever was not measured experimentally; instead, the values reported by the manufacturer were used. Normal forces measured with 3 different AFM tips were calculated and averaged by monitoring force curves in contact mode.

III. Results and Discussion

Design of the LSPR Nanobiosensor. NSL was used to create massively parallel arrays of Ag nanotriangles on a mica substrate, as shown in Figure 1A. AFM studies indicate that these nanotriangles have perpendicular bisectors of ~90 nm and out-of-plane heights of ~50 nm. A self-assembled monolayer (SAM) of 1:3 1-MUA (Figure 1B-1):1-OT (Figure 1B-2) was formed on the surface by incubation for 24 h. An EDC linker was then used to covalently link B (Figure 1B-3) to the carboxylate groups. Given the binding efficiency of EDC, B surface coverage is estimated to be ~1−5% resulting in only 60−300 B molecules per nanoparticle.[45] Figure 1C provides a schematic representation of the binding of AB to biotinylated Ag nanoparticles.

Each step of the functionalization of the samples was monitored using UV−vis spectroscopy, as shown in Figure 2. For simplicity, a positive (+) wavelength shift indicates a red-shift and a negative (−) wavelength shift indicates a blue-shift. These wavelength shifts are monitored and are more reliable than intensity-based measurements. After a 24 h incubation in SAM, the LSPR extinction wavelength of the Ag nanoparticles was measured to be 670.3 nm (Figure 2A). Samples were then incubated for 3 h in B to ensure that the amide bond between the amine and carboxyl groups had been formed. The LSPR wavelength shift due to this binding event was measured to be +12.7 nm, resulting in a LSPR extinction wavelength of 683.0 nm (Figure 2B). At this stage, the nanosensor was ready to detect the specific binding of AB. Incubation in 700 nM AB for 3 h resulted in a LSPR wavelength shift of +42.6 nm, giving a λ_{max} of 725.6 nm (Figure 2C).[45]

Monitoring of the Specific Binding of AB to B and the LSPR Response as a Function of AB Concentration. The

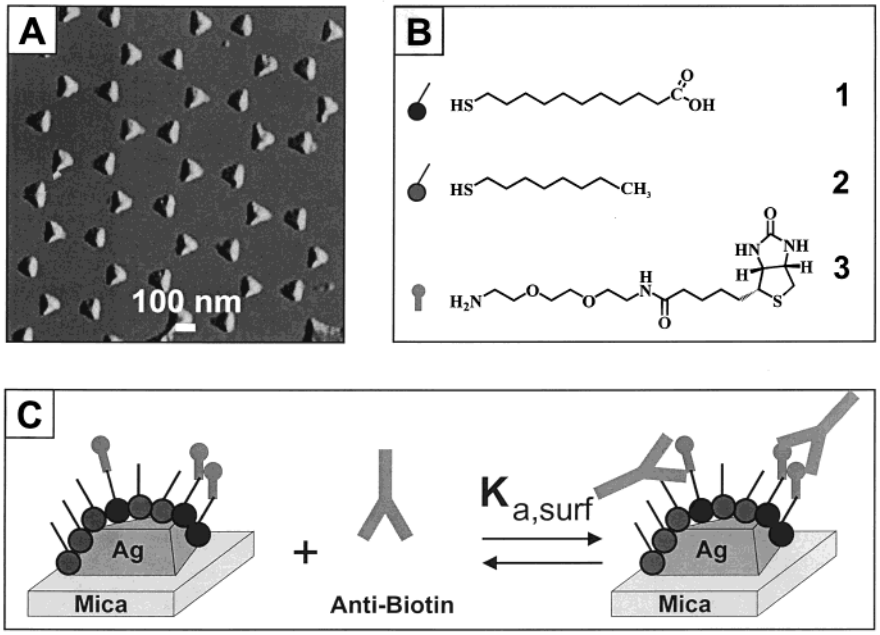

Figure 1. LSPR nanobiosensor. (A) Tapping mode AFM image of the Ag nanoparticles (nanosphere diameter, $D = 390$ nm; mass thickness, $d_m = 50.0$ nm Ag on a mica substrate). Scan area, 3.0 μm^2. Scan rate between 1 and 2 Hz. After solvent annealing, the resulting nanoparticles have in-plane widths of ~100 nm and out-of-plane heights of ~51 nm. (B) Surface chemistry of the Ag nanobiosensor. A mixed monolayer of (1) 11-MUA and (2) 1-OT is formed on the exposed surfaces of the Ag nanoparticles followed by the covalent linking of (3) biotin (B) to the carboxyl groups of (1) 11-MUA. (C) Schematic representation of anti-biotin (AB) binding to a biotinylated Ag nanobiosensor fabricated by NSL on a mica substrate.

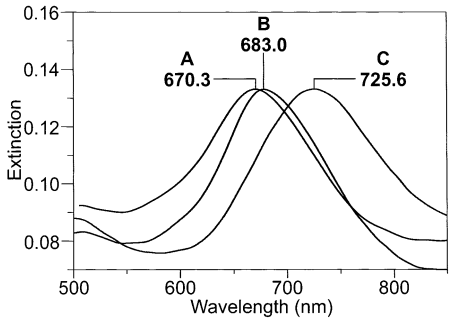

Figure 2. Smoothed LSPR spectra for each step of the preparation of the Ag nanobiosensor, and the specific binding of AB to B. (A) Ag nanoparticles after modification with 1 mM 3:1 1-OT/11-MUA, $\lambda_{max} = 670.3$ nm, (B) Ag nanoparticles after modification with 1 mM B, $\lambda_{max} = 683.0$ nm, and (C) Ag nanoparticles after modification with 700 nM AB, $\lambda_{max} = 725.6$ nm. All spectra were collected in a N_2 environment.

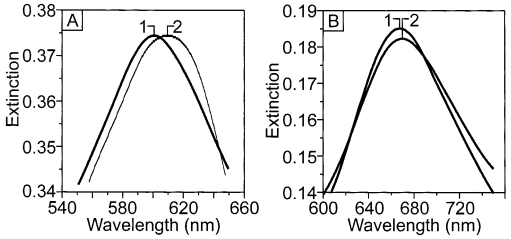

Figure 3. Smoothed LSPR spectra illustrating the response of the Ag nanobiosensor to [AB] corresponding to saturation coverage and limit of detection. All extinction measurements were collected in a N_2 environment. (A) Ag nanoparticles (1) before ($\lambda_{max} = 600.8$ nm) and (2) after ($\lambda_{max} = 638.1$ nm) 7 μM AB exposure. (B) Ag nanoparticles (1) before ($\lambda_{max} = 667.3$ nm) and (2) after ($\lambda_{max} = 669.8$ nm) 700 pM AB exposure.

LSPR response of the nanobiosensor was evaluated for 700 pM < [AB] < 7 μM**.** The absolute value of the λ_{max} varied from sample to sample; however, it has been shown that the absolute value of the λ_{max} does not affect the response shift of the nanobiosensor.[44,45] The sensitivity of the sensor to these slight changes in the local dielectric environment due to the analyte remain unaffected by the value of λ_{max}. Variations in the λ_{max} value have been attributed to small differences in the local dielectric environment due to the adsorption of a water layer (±20 nm) and slight structural variations from nanoparticle to nanoparticle.[44,45,69] Consequently, only the relative wavelength shift, $\Delta\lambda_{max}$, will be used to monitor the binding of the analyte.

The effect of AB concentration on the LSPR response can be seen in Figure 3. The λ_{max} of a biotinylated sample was measured to be 600.8 nm (Figure 3A-1). Exposure of the sample to 7 μM AB produces a LSPR response of +37.3 nm, with a final λ_{max} of 638.1 nm (Figure 3A-2). This wavelength shift results from a maximum AB coverage. Exposure of the sample to 700 pM AB produces a small but reproducible LSPR response shift of + 2.5 nm from 667.3 to 669.8 nm (Figure 3B). This wavelength shift corresponds to the smallest detectable shift for this binding system.

A normalized response curve was then constructed by measuring relative LSPR wavelength shifts after exposure of the biotinylated surface to concentrations of AB between 700 pM and 7 μM, and dividing by the average maximum response ΔR_{max} (Figure 4). Each data point resulted from the analysis of a different sample. Furthermore, since $\Delta\lambda_{max}$ varied slightly (less than ±5 nm) from sample to sample, for each concentration of AB, a minimum of three measurements were performed and the values reported are averages from the various samples. This error is comparable to that seen with other surface-based optical biosensors.[64]

The binding curve provides three important characteristics that describe the binding of AB to B. First, the saturation response and saturation AB concentration can be determined. Fits to the data indicate that the saturation response of the nanobiosensor is 38.0 nm and that saturation begins around 700 nM AB. These results could be refined by obtaining data points

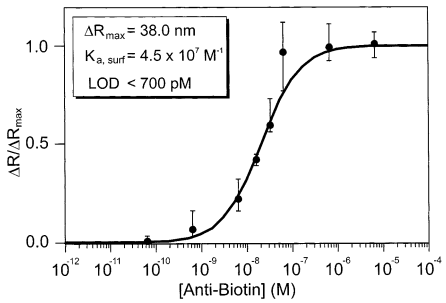

Figure 4. Normalized LSPR shift, $\Delta R/\Delta R_{max}$ versus [AB] response curve for the specific binding of AB to a biotinylated Ag nanobiosensor. All measurements were collected in a N_2 environment. The solid line is the calculated value of $\Delta R/\Delta R_{max}$ using eq 6. Error bars display the total spread in the data collected.

at concentrations much higher than the saturation value; however, this was impossible because the AB was received as a 7 μM solution, the maximum concentration used in this study. The second important characteristic determined by the binding curve is the LOD of the nanobiosensor. In this case, it is estimated that the LOD is <700 pM AB. This number is determined from the detection limits of the detector, the nonspecific response of the LSPR sensor, and the smallest measurable response from the concentrations studies. Finally, the response curve yielded a surface binding constant of 4.5×10^7 M^{-1} for the interaction of B and AB, which falls in the accepted range found in the literature.[37,39] As predicted,[45] the LOD of the nanobiosensor studied is lower for systems with higher binding affinities such as for the well studied biotin−streptavidin couple[70] and higher for systems with lower binding affinities as seen in this B/AB system. The peak-to-peak wavelength shift noise of the baseline in repetitive experiments is ~0.5 nm. Taking the limit of detection as three times this value, one conservatively estimates a LOD of <700 pM. Since the inherent peak-to-peak wavelength shift noise of the miniature CCD spectrometer is ~0.2 nm and this could be improved further by adding temperature control, we anticipate that the signal-to-noise ratio of the LSPR nanobiosensor response could be further improved.

Quantitative Interpretation of the Sensor Response. In a manner analogous to the treatment used by Campbell and coworkers to model SPR spectroscopy[71] and that which was subsequently used as a quantitative interpretation of LSPR biosensors,[45] the LSPR λ_{max} shift response, ΔR in nm, is given by

$$\Delta R = m\,\Delta n_{eff} \tag{1}$$

where m is the refractive index sensitivity of the NSL-derived Ag particles that form the LSPR biosensor and n_{eff} is the effective refractive index of the trilayer structure above the nanoparticle surface. The effective refractive index of this structure is determined by integrating the distance-dependent refractive index, $n(z)$, weighted by the square of the electromagnetic field, $E(z)$, from zero to infinity:

$$n_{eff} = \frac{2}{l_d}\int_0^{\infty} n(z)[E(z)]^2\,dz$$

$$n(z) = \begin{cases} n_{SAM},\ 0 \le z \le d_{SAM} \\ \theta n_{AB} + (1-\theta)n_{ext},\ d_{SAM} \le z \le d_{SAM} + d_{AB} \\ n_{ext},\ d_{SAM} + d_{AB} \le z \le \infty \end{cases} \tag{2}$$

where n_{SAM}, n_{AB}, and n_{ext} are the refractive indexes of the SAM layer, AB (or an adjusted refractive index to compensate for incomplete monolayer formation at saturation coverage), and external medium, respectively, and d_{SAM} and d_{AB} are the thicknesses of the SAM and AB layers, respectively. As in previous work,[45] the electromagnetic field is expressed as $E(z) = \exp(-z/l_d)$ where $l_d \sim 5-6$ nm, although it is known that the true field distribution has a more complex form.[65] For $d_{SAM} \le z \le d_{SAM} + d_{AB}$, $n(z)$ is expressed as a weighted average of the refractive index of AB and n_{ext}. The two refractive indexes are weighted according to the fractional coverage of AB, θ, which is given by the Langmuir adsorption isotherm:

$$\theta = \frac{\Gamma_{AB}}{\Gamma_{AB,max}} = \frac{K_{a,surf}[AB]}{1 + K_{a,surf}[AB]} \tag{3}$$

where Γ_{AB} and $\Gamma_{AB,max}$ are the equilibrium and saturation surface excess of AB, respectively, and $K_{a,surf}$ is the surface-confined binding affinity constant. For analyte molecules on the same size scale as the electromagnetic field decay length or larger, this weighting scheme is preferable to that derived in our previous work.[45] To determine the LSPR biosensor response as a function of θ, Δn_{eff} is defined as the following:

$$\Delta n_{eff} = n_{eff}(\theta) - n_{eff}\,(\theta = 0) \tag{4}$$

Evaluation of eq 2 and substitution into eq 1 yields the absolute response of the AB LSPR biosensor:

$$\Delta R = m\theta(n_{AB} - n_{ext})\exp(-2d_{SAM}/l_d)[1 - \exp(-2d_{AB}/l_d)] \tag{5}$$

The maximum sensor response, ΔR_{max}, occurs when $\theta = 1$ and the normalized LSPR response, $\Delta R/\Delta R_{max}$, is given by

$$\frac{\Delta R}{\Delta R_{max}} = \theta = \frac{K_{a,surf}[AB]}{1 + K_{a,surf}[AB]} \tag{6}$$

Therefore, the normalized response of the AB LSPR biosensor is a direct measurement of the fractional surface coverage of AB and, in turn, has the same functional form as the Langmuir adsorption isotherm. Another desirable characteristic of the normalized sensor response is that, unlike the absolute sensor response, it is completely independent of the electromagnetic field distribution around the nanoparticle.

Orientation of the Binding of AB to B. Height changes during the biosensing experiments were monitored using AFM in tapping mode. Representative AFM images of Ag nanoparticles are shown in Figure 5. The average nanoparticle heights listed represent measurements from AFM line scans from 30+ nanoparticles. Figure 5A shows untreated Ag nanoparticles. The average nanoparticle height, as seen in its line scan, is 51.8 nm ± 1.2 nm. After incubation in SAM, a 1.8 nm increase in nanoparticle height was seen, resulting in an average nanoparticle height of 53.6 nm ± 0.34 nm. This height increase is expected for a monolayer of 1-OT on Ag.[72] Next, B was covalently linked to the surface. Because the B surface coverage is low (~1−5%), a height increase of only 0.2 nm was seen (53.8 nm ± 0.81 nm). Finally, after incubation in 70 nM AB, the average nanoparticle height was found to be 59.8 nm ± 2.1 nm, a 6.0 nm height increase.

Previous studies have shown that AB assumes a position with its long axis oriented vertically when its two Fab fragments bind to separate surface-bound B molecules which would yield a 15 nm thick AB monolayer.[37] AB places its long axis horizontally when only one of its Fab fragments binds to a B molecule, resulting in an AB monolayer whose thickness ranges from 4

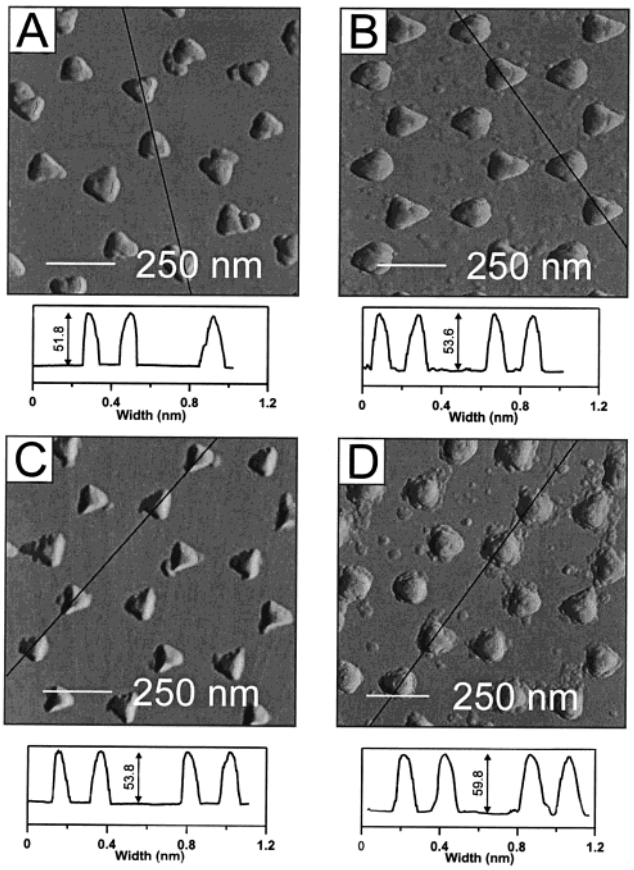

Figure 5. AFM tapping mode studies and line scans to determination the orientation of AB. (A) Unmodified Ag nanoparticles (average height = 51.8 nm), (B) Ag nanoparticles after modification with 3:1 1-OT/11-MUA (average height = 53.6 nm), (C) Ag nanoparticles after modification with B (average height = 53.8 nm), and (D) Ag nanoparticles after modification with a full monolayer of AB (70 nM) (average height = 59.8 nm).

to 10 nm.[73] The experimental value for ΔR_{max} was interpreted in terms of three closest-packed structural models for the surface B−AB complex. The crystal structure for AB has not been determined; however, as a member of the IgG family, its dimensions are approximately $h_{AB} = 4$ nm × $w_{AB} = 10$ nm × $l_{AB} = 15$ nm.[73] The model with l_{AB} oriented horizontally and h_{AB} oriented vertically to the local nanoparticle surface yields a theoretical value for the saturation response, $\Delta R_{max} = 40.6$ nm, in good agreement with experiment, $\Delta R_{max} = 38.0$ nm. The other two models: (1) l_{AB} horizontal and w_{AB} vertical and (2) h_{AB} horizontal and l_{AB} vertical yield theoretical values for the saturation response, $\Delta R_{max} = 53.2$ nm and $\Delta R_{max} = 54.8$ nm, respectively, that are in significantly poorer agreement with experiment. By increasing the concentration of EDC during B linking, the surface coverage of B will increase, thus forcing AB into a vertical configuration. As a result, the LSPR response should increase, thereby increasing the sensitivity of the device.

Measurements of Nanoparticle Adhesion As Determined by AFM. Previous studies using LSPR nanosensors[45] to detect biomolecules used Ag nanoparticles on a piranha-cleaned glass substrate**.** At times, the majority of Ag nanoparticles came off the glass substrate in the presence of water. Combination of the use of mica substrates and addition of surfactant during sphere packing allowed us to combat this problem, thus producing more robust samples.

Using AFM, force calibration plots were used to determine the mechanical stability or adhesion properties of the nanoparticles to glass and mica substrates.[74] On a 1 μm^2 area, the normal force was increased incrementally until the nanoparticles in this square area were completely removed. Contact or tapping mode images at a higher scan size were then collected to show the contrast between the damaged area where elevated forces were applied and the rest of the undamaged sample where lower forces were used. While these normal forces are not the actual forces acting on the nanoparticles,[74−76] they do reveal a useful trend in the adhesive forces between the nanoparticles and a given substrate.

The results of this experiment are summarized in Figure 6. A normal force of 10 nN cleared all of the nanotriangles off the glass substrate (Figure 6A), which is comparable to the 15 nN of normal force needed to denature the chemical bond between Pt nanoparticles and a SiO_2 surface.[74] Furthermore, 50 nN of normal force was necessary to remove all the nanoparticles from a mica substrate that had not been treated with surfactant (Figure 6B). It is proposed that the nanoparticles bind more strongly to mica than to glass because of the smoother, and as a result, larger contact area between the nanoparticles and substrate. Additionally, 90 nN of normal force was required to completely clear all nanoparticles from the mica substrate treated with surfactant (Figure 6C), which is a 9-fold increase from the glass substrate and approximately 2-fold increase from the mica substrate (without surfactant). The exact role of the surfactant is unclear. One hypothesis is that water seeps underneath the nanoparticles and delaminates them from the surface. We believe that the surfactant molecules collect underneath the Ag nanoparticles, preventing the adverse effects of water. Subsequently, this increased nanoparticle adhesion will allow LSPR sensor detection in flowing buffer conditions.

Effectiveness of the LSPR Biosensor in Physiological Conditions. The previous study of streptavidin binding to biotinylated Ag nanoparticles were conducted exclusively in a N_2 environment.[45] However, in order for LSPR nanobiosensors to fulfill their mandate, they must be biocompatible and work under physiological conditions. To emulate physiological conditions, the previously described AB experiment was performed in a 10 mM PBS environment in addition to a N_2 environment with all other parameters held constant.

These results are summarized in Figure 7. In N_2, the observed LSPR wavelength shift due to the addition of 20 nM AB was +16.1 nm, while in a 10 mM PBS environment the LSPR wavelength shift due to the addition of 20 nM AB was +10.0 nm. Theory predicts that the LSPR wavelength shift in 10 mM PBS should be 40% of the shift in N_2, which in this case would correspond to a +6.5 nm shift.[45] However, the shift observed in buffer is about one and one-half times larger than predicted. The fact that the LSPR response depends not only on the local refractive index of the system but also on the orientation of the AB molecules involved in the experiment may explain this result. Even though the buffered solution reduces the refractive index difference between the biomolecule and its environment (in comparison to N_2), the presence of buffer could make the AB molecules more mobile, allowing them to assume a more vertical orientation as described above, thus increasing the LSPR response.

Reversibility of the Interaction Between B and AB. Some binding interactions such as poly-L-lysine to a negatively charged surface can interact reversibly,[44] while other couples with higher surface binding affinities interact irreversibly.[45] A commercially viable nanobiosensor should be entirely reusable. In the case of this study, this means that the layer of analyte, AB, must be entirely removable, leaving the nanoparticles

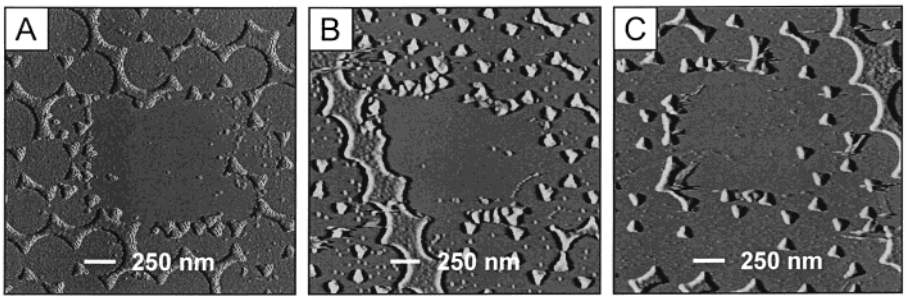

Figure 6. Measurement of the adhesion of Ag nanoparticles (a = 90 nm, b = 50.0 nm) to mica and glass substrates. (A) An AFM image of Ag nanoparticles on a glass substrate. All the nanoparticles in the center 1 μm^2 area were removed after applying 10 nN of normal force to the substrate. The nanoparticles outside this region were not displaced because a lower force was used. (B) An AFM image of Ag nanoparticles on a mica substrate (without surfactant). All the nanoparticles in the center 1 μm^2 area were removed after applying 50 nN of normal force to the substrate. The nanoparticles outside this region were not displaced because a lower force was used. (C) An AFM image of Ag nanoparticles on a mica substrate (with surfactant). All the nanoparticles in the center 1 μm^2 area were removed after applying 90 nN of normal force to the substrate. The nanoparticles outside this region were not displaced because a lower force was used.

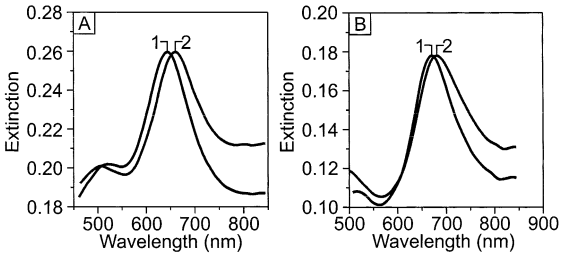

Figure 7. Comparison of AB shifts in N_2 and 10 mM PBS environments (A) Smoothed LSPR spectra showing the LSPR wavelength response shift due to AB in a N_2 environment. (1) Ag nanoparticles after modification with 1 mM B, λ_{max} = 644.2 nm. (2) Ag nanoparticles after modification with 20 nM AB, λ_{max} = 660.3 nm. (B) Smoothed LSPR spectra showing the LSPR wavelength response shift due to AB in 10 mM PBS. (1) Ag particles after modification with 1 mM B, λ_{max} = 671.0 nm, (2) Ag nanoparticles after modification with 20 nM AB, λ_{max} = 681.0 nm.

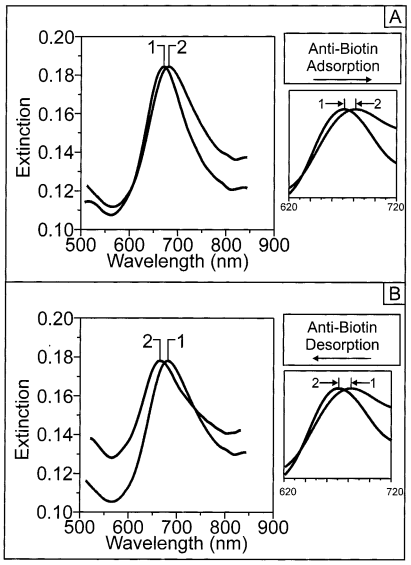

Figure 8. Smoothed LSPR spectra showing the adsorption/desorption of 20 nM AB to biotinylated Ag nanoparticles. (A) AB adsorption: (1) LSPR spectrum of biotinylated Ag nanoparticles in 10 mM PBS, λ_{max} = 671.1 nm, (2) LSPR spectrum of Ag nanoparticles after incubation in 20 nM AB in 10 mM PBS, λ_{max} = 681.8 nm. (B) AB desorption: (1) LSPR spectrum of biotinylated Ag nanoparticles after incubation in 20 nM anti-biotin in 10 mM PBS, λ_{max} = 681.8 nm, (2) LSPR spectrum of Ag nanoparticles after incubation in an excess of B (1 mM) in 10 mM PBS for 30 s, λ_{max} = 670.2 nm.

functionalized with B and ready for additional measurements. Reusability has a large impact on cost-effectiveness and the simplicity of use of biosensors.

The reversibility of the binding between AB and B was tested experimentally by treating samples previously exposed to AB with an excess of concentrated B (1 mM in 10 mM PBS). As hypothesized above, on average, only half of the AB Fab fragments bind to B molecules, thus the excess B can attach to the available Fab sites and rip off the majority of the analyte. The LSPR spectra of a sample before treatment with AB revealed a λ_{max} = 671.1 nm (Figure 8A-1). After incubation in 20 nM AB for 3 h, the LSPR extinction wavelength was λ_{max} = 681.8 nm, a shift of +10.7 nm (Figure 8A-2). After 30 s of exposure to the 1 mM B solution, the LSPR extinction wavelength λ_{max} dropped back to 670.2 nm, a shift of −11.6 nm (Figure 8B). Considering sensor limitations, this value of λ_{max} is essentially identical to its value before treatment with AB, suggesting that the analyte layer had been completely removed. All measurements were made in 10 mM PBS to ensure the applicability of the results to biological sensing. To fully understand this phenomenon, real time kinetic studies of the binding and desorption of AB and the adsorption of B to the nanoparticle surface must be performed. The time scale for these events appears to be less than a minute, except for the coupling of EDC, which is significantly slower. Such studies would also reveal useful kinetic data about the interaction of B and the analyte,[42,77−79] and would provide a supplementary tool to measure the surface binding affinity between the two.

IV. Conclusions

This study provides evidence that triangular Ag nanoparticle LSPR biosensors are applicable to real world conditions, and that these LSPR biosensors have been optimized for strength, reusability, and in vivo applicability. Furthermore, it has been demonstrated that Ag nanoparticle biosensors retain most of the qualities of conventional SPR, by providing sensitive and selective monitoring of binding of an analyte to a nanoparticle surface.

Four major courses of study provided these encouraging results. First, we studied the effect of AB concentration on the nanobiosensor response, and constructed a normalized response curve. Quantitative interpretations of the experimental data showed the following: (1) the maximum LSPR response for the B/AB model was +38.0 nm, (2) the surface-confined thermodynamic binding constant was 4.5 × 10^7 M^{-1}, and (3) the LOD of the sensor was inferior to 700 pM AB. Next, we proved that by using mica as a substrate instead of glass and

by adding a Triton X-100 surfactant during sphere packing, the adhesion of the Ag nanotriangles could be increased by a factor of 9. On surfactant-treated mica samples, a normal force of 90 nN was necessary to remove the nanoparticles from the surface. It was then found that the Ag nanotriangle LSPR biosensor could be used in a buffer solution, a physiological fluid emulate, with less than a 50% decrease in LSPR wavelength response. Additionally, by treating used samples with an excess of 1 mM B solution, it was demonstrated that the binding of AB to the biotinylated surface can be reversed, returning the plasmon to its original value before treatment with AB. Finally, information about the binding orientation of AB to a biotinylated surface was derived from the biosensing studies. It was proved by AFM height studies that the majority of AB molecules position their long axes horizontally, yielding an average height due to AB of 6.0 nm. This indicates that the majority of AB molecules are bound by a single Fab fragment to one surface B molecule. However, it appears that running the experiment in a buffer solution increases the mobility of the antibodies and allows a larger number of them to assume a vertical orientation.

Our results suggest that soon, Ag nanotriangle biosensors could be used for the detection of a wide variety of biomolecules. Binding of DNA,[80] proteins,[32] and possibly eukaryotic cells (by using protein ligand intermediates) to noble metal nanoparticles opens a window of opportunity in medical diagnostics and could greatly simplify often tedious immunohistochemical detection tasks[81] performed regularly in biomedical research. Future work on miniaturization of the sensor, linkage of the sensor to drug delivery chips, and biocompatibility could make this laboratory-based device into a portable diagnostic tool. The simplicity, durability, and reusability of the LSPR nanobiosensor announce its potential use as an affordable and efficient medical device.

Acknowledgment. The authors gratefully acknowledge financial support from the Nanoscale Science and Engineering Initiative of the National Science Foundation under NSF Award EEC-0118025. A. Haes acknowledges the American Chemical Society, Division of Analytical Chemistry sponsored by Eastman Chemical for fellowship support. J. Riboh acknowledges the Nanoscale Science and Engineering Center at Northwestern University, Research Experience for Undergraduates program that is funded under Award EEC-0118025. Any opinions, findings, and conclusions or recommendations expressed in this material are those of the authors and do not necessarily reflect those of the National Science Foundation.

References and Notes

(1) Shipway, A. N.; Katz, E.; Willner, I. *Chem. Phys. Chem.* **2000**, *1*, 18.
(2) Niemeyer, C. M. *Angew. Chem., Int. Ed.* **2001**, *40*, 4128.
(3) Benedek, G.; Martin, T. P.; Pacchioni, G. *Elemental and Molecular Clusters*; Springer Series in Materials Science ed.; Springer-Verlag: Berlin, 1988; Vol. 6.
(4) Alivisatos, A. P. *J. Phys. Chem.* **1996**, *100*, 13226.
(5) Alivisatos, A. P. *Science* **1996**, *271*, 933.
(6) *Clusters and Colloids From Theory to Applications*; Schmid, G., Ed.; VCH Publishers: New York; Weinheim (Federal Republic of Germany), 1994; p 555.
(7) Steigerwald, M. L.; Brus, L. E. *Acc. Chem. Res.* **1990**, *23*, 183.
(8) Brus, L. E.; Szajowski, P. F.; Wilson, W. L.; Harris, T. D.; Schuppler, S.; Citrin, P. H. *J. Am. Chem. Soc.* **1995**, *117*, 2915.
(9) Reed, M. A.; Kirk, W. P. *Nanostructures and Mesoscopic Systems*; Academic Press, Inc.: San Diego, 1991.
(10) Sundaram, M.; Chalmers, S. A.; Hopkins, P. F.; Gossard, A. C. *Science* **1991**, *254*, 1326.
(11) Kreibig, U. Optics of nanosized metals. In *Handbook of Optical Properties*; Hummel, R. E., Wissmann, P., Eds.; CRC Press: Boca Raton, 1997; Vol. 2; p 145.
(12) Kreibig, U.; Gartz, M.; Hilger, A. *Ber. Bunsen-Ges.* **1997**, *101*, 1593.
(13) Kreibig, U.; Gartz, M.; Hilger, A.; Hovel, H. Optical investigations of surfaces and interfaces of metal clusters. *Adv. Met. Semicond. Clusters* **1998**, *4*, 345.
(14) Haynes, C. L.; Van Duyne, R. P. *J. Phys. Chem. B* **2001**, *105*, 5599.
(15) Mulvaney, P. *MRS Bull.* **2001**, *26*, 1009.
(16) El-Sayed, M. A. *Acc. Chem. Res.* **2001**, *34*, 257.
(17) Link, S.; El-Sayed, M. A. *J. Phys. Chem. B* **1999**, *103*, 8410.
(18) Mulvaney, P. *Langmuir* **1996**, *12*, 788.
(19) Jensen, T. R.; Kelly, K. L.; Lazarides, A.; Schatz, G. C. *J. Cluster Sci.* **1999**, *10*, 295.
(20) Jensen, T. R.; Malinsky, M. D.; Haynes, C. L.; Van Duyne, R. P. *J. Phys. Chem. B* **2000**, *104*, 10549.
(21) Michaels, A. M.; Nirmal, M.; Brus, L. E. *J. Am. Chem. Soc.* **1999**, *121*, 9932.
(22) Schultz, S.; Smith, D. R.; Mock, J. J.; Schultz, D. A. *P. N. A. S.* **2000**, *97*, 996.
(23) Yguerabide, J.; Yguerabide, E. E. *Anal. Biochem.* **1998**, *262*, 137.
(24) Yguerabide, J.; Yguerabide, E. E. *Anal. Biochem.* **1998**, *262*, 157.
(25) Schatz, G. C.; Van Duyne, R. P. *Electromagnetic Mechanism of Surface-Enhanced Spectroscopy*; Wiley: New York, 2002; Vol. 1.
(26) Turner, A. P. F. *Science* **2000**, *290*, 1315.
(27) Iwasaki, Y.; Horiuchi, T.; Niwa, O. *Anal. Chem.* **2001**, *73*, 1595.
(28) Maxwell, D. J.; Taylor, J. R.; Nie, S. *J. Am. Chem. Soc.* **2002**, *124*, 9606.
(29) Ivansson, D.; Bayer, K.; Mandenius, C. F. *Anal. Chim. Acta* **2002**, *456*, 193.
(30) Spangler, B. D.; Wilkinson, E. A.; Murphy, J. T.; Tyler, B. J. *Anal. Chim. Acta* **2001**, *444*, 149.
(31) Ligler, F. S.; Goldn, J. P.; Shriver Lake, L. C.; Ogert, R. A.; Wijesuria, D.; Anderson, G. P. *ImmunoMethods* **1993**, *3*, 122.
(32) Copeland, R. A.; Fodor, S. P. A.; Spiro, T. G. *J. Am. Chem. Soc.* **1984**, *106*, 3872.
(33) Suzuki, M.; Ozawa, F.; Wakako, S.; Aso, S. *Anal. Bioanal. Chem.* **2002**, *372*, 301.
(34) *Immunoassay*; Diamandis, E. P., Christopoulos, T. K., Eds.; Academic Press: San Diego, CA, 1996.
(35) Williams, A. F.; Barclay, A. N. *Annu. Rev. Immunol.* **1988**, *6*, 381.
(36) Silverton, E. W.; Navia, M. A.; Davies, D. R. *Proc. Natl. Acad. Sci.* **1977**, *74*, 5140.
(37) Lynch, N. J.; Kilpatrick, R. K.; Carbonell, R. G. *Biotechnol. Bioeng.* **1996**, *50*, 169.
(38) Coille, I.; Gauglitz, G.; Hoebeke, J. *Anal. Bioanal. Chem.* **2002**, *372*, 293.
(39) Adamczyk, M.; Mattingly, P. G.; Shreder, K.; Yu, Z. *Bioconjugate Chem.* **1999**, *10*, 1032.
(40) Cui, Y.; Wei, Q.; Park, H.; Lieber, C. M. *Science* **2001**, *293*, 1289.
(41) Kim, S. R.; Abbot, N. L. *Adv. Mater.* **2001**, *13*, 1445.
(42) Schuck, P. *Annu. Rev. Biophys. Biomol. Struct.* **1997**, *26*, 541.
(43) Blake, R. C.; Pavlov, A. R.; Blake, D. A. *Anal. Biochem.* **1999**, *272*, 123.
(44) Malinsky, M. D.; Kelly, K. L.; Schatz, G. C.; Van Duyne, R. P. *J. Am. Chem. Soc.* **2001**, *123*, 1471.
(45) Haes, A. J.; Van Duyne, R. P. *J. Am. Chem. Soc.* **2002**, *124*, 10596
(46) Lee, H. J.; Goodrich, T. T.; Corn, R. M. *Anal. Chem.* **2001**, *73*, 5525.
(47) Hall, D. *Anal. Biochem.* **2001**, *288*, 109.
(48) Wang, J.; Cai, X.; Rivas, G.; Shiraishi, H.; Farias, P. A. M.; Dontha, N. *Anal. Chem.* **1996**, *68*, 2629.
(49) Walterbeek, H. T.; van der Meer, A. J. G. M. *J. Environ. Radioact.* **1996**, *33*, 237.
(50) Thevenot, D. R.; Toth, K.; Durst, R. A.; Wilson, G. S. *Biosens. Bioelectron.* **2001**, *16*, 121.
(51) Mascini, M.; Palchetti, I.; Marrazza, G. *Fresenius' J. Anal. Chem.* **2001**, *369*, 15.
(52) Horacek, J.; Skladal, P. *Anal. Chim. Acta* **1997**, *347*, 43.
(53) Ebersole, R. C.; Miller, J. A.; Moran, J. R.; Ward, M. D. *J. Am. Chem. Soc.* **1990**, *112*, 3239.
(54) Miller, M. M.; Sheehan, P. E.; Edelstein, R. L.; Tamanaha, C. R.; Zhong, L.; Bounnak, S.; Whitman, L. J.; Colton, R. J. *J. Magn. Magn. Mater.* **2001**, *225*, 156.
(55) Chemla, Y. R.; Grossman, H. L.; Poon, Y.; McDermott, R.; Stevens, R.; Alper, M. D.; Clarke, J. *Proc. Natl. Acad. Sci.* **2000**, *97*, 26.
(56) Raiteri, R.; Grattarola, M.; Butt, H.-J.; Skladal, P. *Sens. Actuators, B* **2001**, *B79*, 115.
(57) Kasemo, B. *Curr. Opin. Solid State Mater. Sci.* **1998**, *3*, 451.
(58) Natsume, T.; Nakayama, H.; Isobe, T. *Trends in Biotech.* **2001**, *19*, S28.
(59) Polla, D. L.; Erdman, A. G.; Robbins, W. P.; Markus, D. T.; Diaz-Diaz, J.; Rizq, R.; Nam, Y.; Brickner, H. T.; Wang, A.; Krulevitch, P. *Annu. Rev. Biomed. Eng.* **2000**, *2*, 551.

(60) Brockman, J. M.; Nelson, B. P.; Corn, R. M. *Annu. Rev. Phys. Chem.* **2000**, *51*, 41.
(61) Berger, C. E. H.; Beumer, T. A. M.; Kooyman, R. P. H.; Greve, J. *Anal. Chem.* **1998**, *70*, 703.
(62) Karlsson, R.; Stahlberg, R. *Anal. Biochem.* **1995**, *228*, 274.
(63) Zizlsperger, M.; Knoll, W. *Prog. Colloid Polymer Sci.* **1998**, *109 (Horizons 2000*— Aspects of Colloid and Interface Science at the Turn of the Millenium), 244.
(64) Smith, E. A.; Erickson, M. G.; Ulijasz, A. T.; Weisblum, B.; Corn, R. M. *Langmuir* **2002**, *ASAP*.
(65) Haes, A. J.; Kelly, K. L.; Schatz, G. C.; Van Duyne, R. P. To be published.
(66) Jensen, T. R.; Schatz, G. C.; Van Duyne, R. P. *J. Phys. Chem. B* **1999**, *103*, 2394.
(67) Starr, C.; Taggart, R. *Biology, The United and Diversity of Life*, 7th ed.; Wadsworth Publishing Company: Belmont, CA, 1995.
(68) Sonnichsen, C.; Geier, S.; Hecker, N. E.; von Plessen, G.; Feldmann, J.; Ditlbacher, H.; Lamprecht, B.; Krenn, J. R.; Aussenegg, F. R.; Chan, V. Z.-H.; Spatz, J. P.; Moller, M. *Appl. Phys. Lett.* **2000**, *77*, 2949.
(69) Haynes, C. L.; Van Duyne, R. P. Submitted.
(70) Green, N. M. *Adv. Protein Chem.* **1975**, *29*, 85.
(71) Jung, L. S.; Campbell, C. T.; Chinowsky, T. M.; Mar, M. N.; Yee, S. S. *Langmuir* **1998**, *14*, 5636.
(72) Walczak, M. M.; Chung, C.; Stole, S. M.; Widrig, C. A.; Porter, M. D. *J. Am. Chem. Soc.* **1991**, *113*, 2370.
(73) Kim, S. R.; Abbott, N. L. *Langmuir* **2002**, *18*, 5269.
(74) Eppler, A. S.; Rupprechter, G.; Anderson, E. A.; Somorjai, G. A. *J. Phys. Chem. B* **2000**, *104*, 7286.
(75) Ogletree, D. F.; Carpick, R. W.; Salmeron, M. *Rev. Sci. Instrum.* **1996**, *67*, 3298.
(76) Frink, L. J. D.; vanSwolf, F. *J. Chem. Phys.* **1997**, *106*, 3782.
(77) Jung, L. S.; Campbell, C. T. *Phys. Rev. Lett.* **2000**, *84*, 5164.
(78) Jung, L. S.; Campbell, C. T. *J. Phys. Chem. B* **2000**, *104*, 11168.
(79) Frey, B. L.; Corn, R. M. *Anal. Chem.* **1996**, *68*, 3187.
(80) Cao, Y. W.; Jin, R.; Mirkin, C. A. *J. Am. Chem. Soc.* **2001**, *123*, 7961.
(81) Freedman, L. J.; Maddox, M. T. *J. Neuro. Methods* **2001**, *112*, 43.